Journal of Membrane Science 719 (2025) 123725

Contents lists available at ScienceDirect

Journal of Membrane Science

journal homepage: www.elsevier.com/locate/memsci

Determining UF hollow fiber membrane integrity with novel microbial monitoring method

Dwani Venkataswamy Gowda [a,*], Danny Harmsen [b], Stefan Koel [c], Han Vervaeren [d], Arnout D'Haese [a], Emile R. Cornelissen [a,b]

[a] Ghent University, Particle and Interfacial Technology Group, Coupure Links 653, 9000, Ghent, Belgium
[b] KWR Watercycle Research Institute, Groningenhaven 7, 3433, PE, Nieuwegein, the Netherlands
[c] Pentair X-Flow BV, Marssteden 50, P.O. Box 741, 7500, AS, Enschede, the Netherlands
[d] De Watergroep, Vooruitgangstraat 189, 1030, Brussels, Belgium

A B S T R A C T

This study presents the Natural Virus (NV) method, a novel approach for monitoring the integrity of ultrafiltration (UF) hollow fiber membranes by quantifying naturally occurring viruses in surface water. The method was applied across laboratory, pilot, and full-scale UF systems to evaluate the impact of fiber integrity on virus removal and provided critical maintenance input for operation. In a laboratory-scale test with a 120-fiber module, a single damaged fiber reduced the removal efficiency from an intact value of LRV 5 to as low as LRV 1, depending on the nature of the damage (fiber breakage or fiber leak), which affected flow rates and permeate concentrations. Pilot-scale tests with an 8" UF module demonstrated the potential for full integrity restoration by re-plugging damaged fibers. At full scale, the NV method exhibited high sensitivity to module integrity, with log removal values (LRVs) ranging from 1.8 to 5. A predictive model, developed based on permeability data and flow dynamics calculations, showed a strong correlation with experimental results, enabling estimation of the number of damaged fibers based on observed LRV. Critical LRV thresholds for maintenance were established: compromised performance ($2.9 \geq$ LRV >2.3) suggesting consideration of fiber re-plugging, and critical performance (LRV ≤ 2.3) indicating the need for module replacement. The NV method demonstrated superior sensitivity compared to conventional techniques like turbidity measurements, proving effective at all tested scales.

1. Introduction

With the increasing number of studies aimed at achieving global sanitation and clean water goals, such as those outlined in the Sustainable Development Goals (SDG6) or the WASH initiative, there is a growing emphasis on ensuring safe drinking water and the consequences of failures in water treatment efficiency and distribution networks [1–3]. Outbreaks of waterborne diseases continue to affect large populations in developing countries, such as India and Bangladesh [4–6], but even developed nations are not immune to these risks in recent years [7,8]. For example, in 2019, Askoy, Norway, reported a gastroenteritis outbreak caused by campylobacter contamination in the water supply, which was traced back to an aging infrastructure [9]. Similarly, in Muxia, Spain, in 2021, a norovirus GII.3 outbreak linked to chlorination failure at a treatment plant, leading to the distribution of contaminated drinking water [10]. These cases highlight the importance of well-maintained water systems, robust operational and maintenance practices, and reliable early warning monitoring to prevent contamination. European legislation for water reuse and drinking water now emphasizes the implementation of a risk assessment approach related to the performance of the installation [11].

Hollow fiber ultrafiltration (UF) membranes are increasingly used in water production centers (WPCs) as a physical barrier for disinfection, due to their ability to retain microbial contaminants, e.g. bacteria, and viruses, through size exclusion mechanisms [12,13]. Despite their strong mechanical properties [14], operational data and research show that fiber breakage occurs in practice [15], leading to the passage of microbial contaminants resulting in compromising water quality. Fiber failures can occur as a result of different reasons: a) improper installation [16], b) pressure spikes during operation or backwash leading to excessive movement or fiber snapping but, also excessive movement can be caused at the potting interface due to excess burst pressure [17], c) membrane aging/degradation from cleaning chemicals [18,19] and, d) scouring by particles from inadequate pretreatment [20,21]. Fiber breakage has been estimated at an average rate of one fiber breakage per module per year, out of 10,000–1,000,000 fibers [16].

Various techniques are used to monitor the integrity of UF membranes in WPCs, categorized as direct and indirect methods. Direct

* Corresponding author.
E-mail address: dwani.venkataswamygowda@ugent.be (D.V. Gowda).

https://doi.org/10.1016/j.memsci.2025.123725
Received 11 November 2024; Received in revised form 29 December 2024; Accepted 10 January 2025
Available online 11 January 2025

methods, such as the pressure decay test (PDT) [22], diffusive air flow test (DAF) [23], and bubble point test [24] assess the membrane module directly but often require systems shutdowns. Indirect methods, such as turbidity measurement and particle counting [25], analyze water quality before and after filtration. Despite being available as an online device for real-time monitoring [26,27], indirect methods often lack sensitivity to detect small defects, such as pinholes or direct fiber breaks, which could permit the breakthrough of virus particles ([28]; J. [29]). Alternative monitoring techniques, such as spiking water with non-native compounds like MS-2 phage, fluorescent compounds, or nanoprobes [30–32], raise concerns about introducing contaminants into the water supply. Other newer monitoring methods are constantly being developed and tested for UF membrane monitoring and can be found in the literature [33–35].

While water treatment facilities opt for multibarrier systems for effective risk management, from the monitoring perspective, a regulatory indicator coupled with online monitoring has not been agreed upon for cases where turbidity measurements are insufficient. An overall LRV for viruses and bacteria must be achieved by the treatment facilities contributed by individual processes LRV. At least an LRV of 4 for virus retention is expected for most individual treatments forming the multibarrier approach and thus, a failure in any one of them will affect the overall LRV of the facility.

This study introduces for the first time the application of natural viruses (NV) as indicators for UF membrane integrity monitoring. By quantifying NV concentrations before and after UF treatment using quantitative polymerase chain reaction (qPCR), the method can detect virus concentrations in the range of 10^7-10^8 gene copies/ml in surface water. A detailed description of the method is provided in our previous research [36]. While our previous research focused on reverse osmosis (RO) membranes, this research extends the NV method to UF hollow fiber membranes. We present a comprehensive experimental approach at laboratory, pilot, and full-scale scale to establish the method's sensitivity. Data collected over a year from full-scale plants, combined with lab-scale experiments and predictive modeling, are used to guide pilot-scale experiments and determine fiber breakage on full-scale based on LRV measurements.

In addition, we explore the possibility of extending the service life of UF modules, by re-plugging broken fibers. While polymeric membranes have a theoretical lifespan beyond the recommended 7–10 years [37] ensuring water quality after fiber repairs is a challenge. Using the NV method, we evaluate the integrity of UF modules with broken fibers, repaired, and intact fibers across laboratory, pilot, and full-scale systems. This systematic approach aims to answer where the lifecycle for UF modules can be extended while maintaining high water quality standards.

2. Methods and materials

2.1. Isolation and quantification of viruses from surface water

Isolation and sequencing of viruses from surface water was carried out in our previous work [38]. For this method, 200L of surface water was collected from Lek Canal (Nieuwegein, NL) and concentrated to 0.27 L using cross-flow ultrafiltration with a 10 nm pore size. Sequential filtration with 0.7 μm and 0.22 μm filters was used to remove algae, bacteria, and protozoa. The viruses were further concentrated via ultracentrifugation (Centricon 100 kDa filter) and resuspended in 500 μL of sterile water. Prior to DNA and RNA extraction, the virus suspension was treated with DNAse (2 U μl^{-1}, Invitrogen) at 37 °C for 45 min to degrade any free DNA present. RNA and DNA were then extracted using the Purelink™ Viral RNA/DNA kit. Virus sequencing was performed using the Illumina HiSeq 2500 platform, with data analysis carried out by BaseClear. Four high-coverage scaffolds from DNA virus sequences were chosen for qPCR primer development to detect these viruses in the sample.

In this study, raw surface water samples were collected from three locations - Lek Canal (Niewegein, NL), Twentekanaal (Elsbeekweg, Enschede, NL), and the Kortrijk-Bossuit Canal (dosed with $FeCl_3$, DeGavers WPC facility, BE) - to quantify naturally present virus strains. Two 500 mL samples were collected from each location and concentrated by centrifugation at 3000*g* for 10 min using ultrafiltration filters (Centricon 100 kDa filter). DNA was extracted using the PowerBiofilm™ kit (Qiagen 24,000–50) and eluted in 220 μL of elution buffer. An internal standard was added to assess the efficiency of the extraction process. qPCR was conducted with 5 μL of DNA, 12.5 μL of SYBR-Green mix (Bio-Rad), and primers at a final concentration of 10 μM, following the PCR conditions described by Ref. [38]. Melting curve analysis confirmed the amplification of the correct virus strains, with negative controls (sterile ultrapure water) ensuring the accuracy of the results. Viruses labeled NV2247 and NV2310, based on the primer set used, were the most abundant strains found in all three surface water samples.

2.2. Surface water quality

Three types of surface water were used in this study, based on the location of the planned experiments. The first source was surface water from the Lek Canal (Nieuwegein, NL) collected for the laboratory-scale tests in May 2021. This water was stored at 4 °C, and its quality was tested for the most abundant natural virus strains (NV) and turbidity. NV concentration ranged from 1×10^7 to 5×10^8 gene copies/L, with a turbidity of 13.6 ± 1.7 FNU.

The second source was surface water from the Twentekanaal (Elsbeekweg, Enschede, NL), where the pilot setup was located (October 2021). NV marker concentration ranged from 1×10^8 to 9×10^8 gene copies/L, and the turbidity was measured at 1.57 FNU.

The third source was the surface water from the Kortrijk-Bossuit Canal (De Gavers WPC facility, BE) where full-scale studies were conducted between July 2020 and December 2021. NV concentrations were measured quarterly, ranging from 1×10^6 to 4×10^8 gene copies/mL., with the lower NV concentrations recorded in December 2020. Turbidity measurements for this source were not recorded.

2.3. Membrane material

Various UF hollow fiber membranes with a 150 kDa molecular weight cutoff were evaluated in laboratory, pilot, and full-scale settings, as summarized in Table 1. For the lab-scale study, the UF RX300 membrane, containing 120 fibers, was used. In the pilot-scale study, the X-Flow Aquaflex 64 membrane, with 18360 fibers in 8" modules, was used. Over twelve months at the WPC De Gavers facility, measurements were carried out on three UF blocks equipped with Pentair X-Flow Aquaflex 40 membranes. During this testing period, two of the three blocks had their UF membranes replaced with new X-Flow Aquaflex 64 after ten years of operation.

Table 1
Membrane specifications.

Name	UF RX300	X-Flow Aquaflex 40	X-Flow Aquaflex 64
Material	Polyethersulfone	Polyethersulfone	Polyethersulfone
Molecular Weight Cutoff	150 kDa	150 kDa	150 kDa
No. of fibers	120	11000	18360
Membrane area	0.08 m^2	40 m^2	64 m^2
Max. temperature	60 °C	40 °C	40 °C
Max. transmembrane pressure	200 kPa (at 30–60 °C)	300 kPa	300 kPa
Mode	Inside-out	Inside-out	Inside-out
Testing	Lab-scale	Full-scale	Pilot-scale/Full-scale

2.4. Membrane damage and repair

The membrane damage protocol varied depending on the type of experiments, as shown in Fig. 1. For lab-scale experiments, two invasive methods were used to damage the UF fibers. In the first method, a 0.5 mm drill hole was made in an intact fiber, referred to as "leaky fibers", to simulate material disintegration. In the second method, fibers were manually shortened using a 1 mm thick scalpel and then potted into custom-made TRX modules to simulate a broken fiber, referred to as "short fibers". In each test, 1 and 3 fibers were damaged separately.

In the pilot-scale setup, individual fibers were cut through access holes engineered into the pressure vessel, referred to as "outlets" to simulate damage. To restore the damaged fibers in the pilot-scale system, a systematic re-plugging method was employed using an insertion tool with ribbed pespin (details of which are not included in this study due to non-disclosure). The experimental schematic, following the sequence of fiber damage, repair, and subsequent fiber re-damage is illustrated in Figure S-1. The damaging tests incrementally damaged fibers in sets of 1, 3, 5, 10, and 50, while the repair process reverse this order. Initially, 40 fibers were repaired, filtration tests were conducted, and samples were taken, followed by the repair of the last 10 fibers. The test set 3 involved repeating the fiber damage procedure, incrementally damaging 2 and 4 fibers.

2.5. Lab scale experimental set-up

Fiber breakage tests were performed on a lab-scale TRX test unit TRX (Pentair, NL) (Figure S-2) with an RX300 membrane module. The characteristics of the RX300 module are listed in Table 1. The test setup facilitates a horizontal installation of the module. The procedure begins by flushing the RX300 module with MilliQ water for at least 20 min in dead-end mode to remove any preservatives from the membranes. For permeability measurements, the RX300 modules are installed in the TRX unit, and the tanks are filled with 5 L of MilliQ water. The pump is turned on to flush the system in cross-flow mode at a feed pressure of approximately 0.5 bar. After about 10 s, the retentate valve is closed, switching the setup to a dead-end module, and the permeate is drained by adjusting the 3-way valve to the drain position. Once the pressure stabilizes, the permeate is collected for 1 min, and its weight is recorded. This data is used to calculate mass flux, and the procedure is repeated for duplicate measurements.

For filtration measurements, the setup is filled with 5L of the surface water, and the same procedure is followed. Once the feed pressure stabilizes at 0.5 bar, the permeate is collected. A total of 4 L of feed is filtered through the module, and a permeate sample is collected. The samples are then processed as previously described and stored for further analysis.

2.6. Pilot-scale experimental setup

The pilot-scale setup, constructed by Pentair X-Flow, operated with an 8-inch Aquaflex 64 module at a flux of 80 L m^{-2} h^{-1} and 0.1–0.2 bar. Three filtration cycles were performed in a dead-end configuration, with each cycle consisting of 20 min of filtration followed by 30 s of hydraulic cleaning to remove any contamination. Forward flushes (15s) and backward flushes (30s) were carried out using feed water. Grab sampling of feed and permeate were collected between the second and third filtration cycles. The tests were carried out with both an intact module and a module with 1, 3, 5, 10, and 50 cut fibers. The grab samples were analyzed for turbidity and stored for later NV sampling.

2.7. Full-scale setup

The water production center (WPC) operated by De Watergroep in Harelbeke, Belgium (Fig. 2) was studied for over a year. The WPC sources surface water from the Bossuit-Kortrijk canal, and its pre-treatment process involves five nitrification reactors that oxidize NH_4^+ to NO_3^- by bacterial activity. Additionally, three flocculators in series, using $FeCl_3$, are used for phosphate removal. After pre-treatment, the water is stored in an artificial pond "De Gavers", which has a storage capacity of 3.2 Mm^3. In the post-treatment step, the water is divided into two fractions: the larger fraction undergoes flocculation to remove suspended solids and reduce turbidity, while the second fraction is sieved (100 μm) and filtered through ultrafiltration skids. Both fractions subsequently mix and pass through activated carbon filters, chlorination step, and then pressurization to be directed to the drinking water mains.

The UF system comprises four skids, each equipped with 40 vertically placed modules, operational since 2011. The skids are designed to accommodate modules from several manufacturers with only minor piping adjustments. In this study, three skids containing single-bore UF membranes (Pentair Aquaflex40), with an internal diameter of 0.8 mm and a total membrane surface of 1600 m^2 per skid are presented. The membranes are operated in an inside-out configuration, with each module having two feed/retentate connectors and one permeate connector. To minimize fouling, measures like chemically enhanced backwash with sodium hydroxide or sulfuric acid (optionally combined with hydrogen peroxide) and cleaning-in-place (CIP) procedures are implemented. The CIP system includes a 5 m^3 tank with a recirculation pump. A detailed description of the WPC installation can be found in a separate study [39].

Throughout the study, permeate samples were collected quarterly from each UF skid's permeate collector. Since feed samples could not be taken directly from the UF skid inlets, pre-treated water from the De Gavers pond was used. In November 2021, after 10 years of operation, the Pentair Aquaflex40 membranes in two skids were replaced with new membrane Pentair Aquaflex64 modules. The impact of this membrane

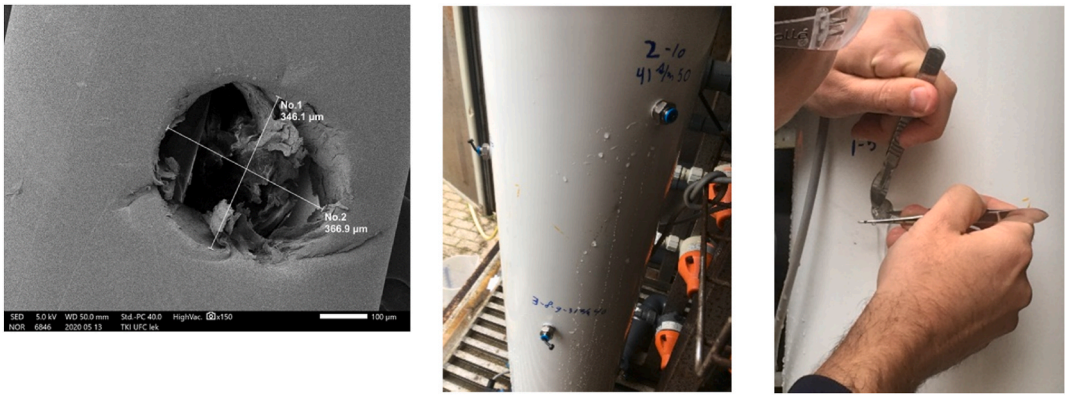

Fig. 1. Fiber damage, left: leaky UF fibers with 0.5 mm drill hole, middle: access outlets in the pressure vessel, left: short UF fiber through cutting.

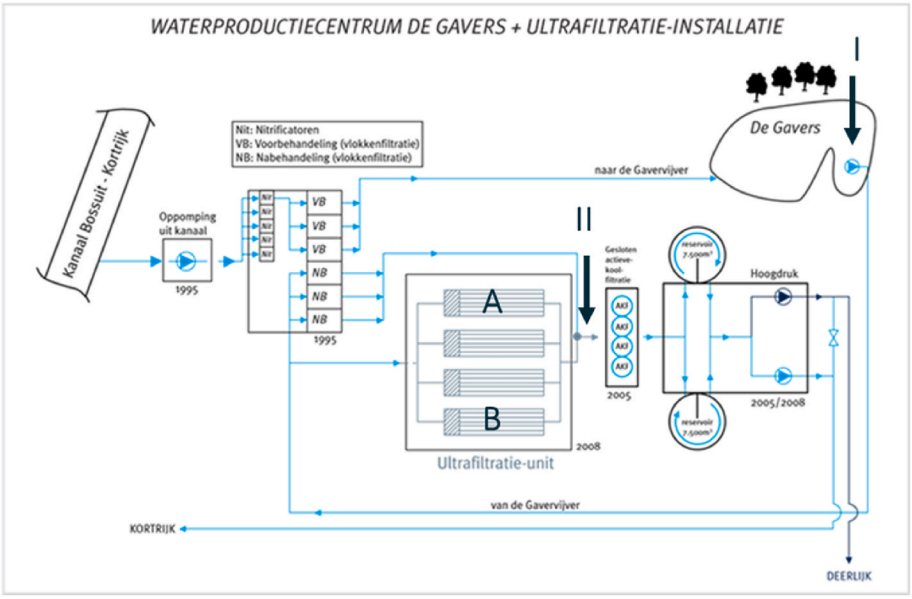

Fig. 2. Water production center at De Gavers, I: De Gavers raw water, II: Permeate after UF skids, A: 3 skids with Pentair membrane, B: skid with Suez membranes.

replacement on NV measurements was analyzed in the study. Only the results from the first three UF skids are presented here.

2.8. Model description for LRV prediction

When a fiber is structurally intact, a significant portion of fluid flow through the fiber can be modeled using conventional methods to either laminar (Re < 2000) or turbulent flow conditions (Re > 4000). For laminar flow, the Hagen-Poiseuille equation [40] is typically used, while the Darcy-Weisbach equation [41] applies to turbulent flow. For laminar flow through an intact fiber, the pressure drop (Δp, bar) across a fiber, as governed by the energy equation, is expressed as:

$$\Delta p = \frac{32\mu L_{eff} V}{d_h^2} \tag{1}$$

Where μ (kg.m^{-1}.s^{-1}) is the dynamic viscosity, L_{eff} (m) is the effective length of the fiber, V (m/s) is the mean velocity (calculated from experimentally obtained average flow rates), and d_h (m) is the hydraulic diameter of the fiber.

After fiber breakage occurs at a distance *s* (m) downstream from the inflow, the flow through the fiber may transition to a turbulent or transitional regime. In such cases, for a given pressure drop, the energy equation Eq (1) changes. For laminar flow, the velocity V can be expressed as:

$$V = \frac{32\mu s}{\alpha\rho d_h^2}\left(\sqrt{1+\frac{\alpha\rho d_h^4}{512\mu^2 s^2}\Delta p} - 1\right) \tag{2}$$

Where ρ (kg/m^3)is the density of water, g (m/s^2) is the acceleration due to gravity and α is a correction coefficient for the kinetic energy and is 2 for laminar flow.

For transitional and turbulent flow (α = 2), the energy equation changes to:

$$V = \sqrt{\frac{2}{\rho}\frac{\Delta p}{\alpha + \frac{fs}{d_h}}} \tag{3}$$

Where, the friction factor f is a function of the Reynolds number, Re [42]. The energy equation must be solved iteratively since f is dependent on V through Re:

For turbulent flow, the relationship is given by:

$$\frac{1}{\sqrt{f}} = 0.8684\ln\left(Re\sqrt{f}\right) - 0.8 \tag{4}$$

Where $Re = Vd_h\rho/\mu$

For the transitional region, the friction factor is described by:

$$f = 0.0115\ln(Re) - 0.0557 \tag{5}$$

The virus retention of an intact fiber is represented by the log reduction value (LRV_i):

$$LRV_i = -\log_{10}\left(\frac{c_{p,i}}{c_f}\right) \tag{6}$$

Where, C_f and C_p are the concentrations of the retained species on the feed and permeate side, respectively.

When the fiber is damaged, the concentration of retained species on the permeate side is significantly affected by changes in the flow rate through the fiber. In such cases, the total flow rate through the fiber affects the species retention. The permeate flow through each fiber (intact or broken) can be expressed by

$$Q = A_{fiber} * Permeability * P \tag{7}$$

$$A_{fiber} = \pi * d_h * L_{eff} \tag{8}$$

Where A_{fiber} (m^2) is the surface area of the fiber, P (bar) is the average pressure. Permeability values for both intact and damaged fibers were obtained experimentally using a lab-scale setup.

In case of a complete fiber breakage, the total flowrate Q_t (m^3/h) through the broken fiber becomes a sum of filtered and unfiltered flow:

$$Q_t = Q_i(N_t - N_d) + Q_d N_d \tag{9}$$

Where Q_i is the flow rate through the intact, Q_d is the flow rate through the damaged fibers. N_t and N_d represent the total number of fibers and the number of broken fibers, respectively. The predicted LRV after fiber breakage can be calculated as follows [43]:

$$LRV_p = \log_{10}\left(\frac{Q_t c_f}{Q_i(N_t - N_d)C_{p,i} + Q_d N_d C_{p,d}}\right) \tag{10}$$

Using Eq (6) for $C_{p,\,i}$ and $C_{p,d}$:

$$LRV_p = -log_{10}\left(\left(\frac{Q_i(N_t - N_d)C_f}{10^{LRV_i}} + \frac{Q_d N_d C_f}{10^{LRV_d}}\right) \Big/ (Q_t C_f)\right) \quad (11)$$

Where LRV_i and LRV_d are the log reduction values of intact fiber and that of damaged fiber, respectively. This LRV_p following fiber breakage, indicates the impact of the LRV of an intact UF module on the reduction in LRV. For large modules with a high number of fibers ($N_t \gg N_d$), Eq (10) can be simplified for N_t-$N_d = N_t$.

3. Results and discussions

3.1. Impact of fiber damage on a lab-scale module

The module consisted of 120 fibers placed vertically, each fiber with an inner diameter (d) of 0.8 mm. The effective length of an individual fiber (L_{eff}) was 0.27 m and the pressure drop over the fiber was 0.01 bar. As water flowed through the fiber, the total flow on the permeate side was 25.3 L/h, resulting in a flow rate of 0.22 L/h through a single intact fiber. The corresponding mean velocity was calculated to be 0.12 m/s and the Reynolds number (Re) = ρVd/μ = was calculated to be 100, where μ and ρ were the viscosity and density of surface water at 20 °C. This confirmed that the flow was laminar, which supports the use of the Hagen-Poiseuille model for calculating the pressure drop. The calculated pressure drop of 0.01 bar aligned with the experimentally recorded pressure drop, further validating the assumption of laminar flow.

During the rejection test (Fig. 3), the intact module demonstrated a high LRV of approximately 5.5 for both NV2247 and NV2310. The turbidity rejection was comparatively lower, achieving an LRV of 2.2, which can be attributed to the lower sensitivity of the quantifying method used. Additionally, the intact module demonstrated a water permeability of 750 L m^{-2} h^{-1}.bar^{-1} at 0.5 bar.

The introduction of fiber damage significantly affected both permeability and virus rejection values. When a single intact fiber was replaced with a leaky fiber (containing a 0.5 mm hole), water permeability increased by 8–10 %, reaching 811.1 L m^{-2} h^{-1}.bar^{-1}. This increase was accompanied by a substantial drop in virus rejection, with LRV_{NV2247} decreasing to 0.89, LRV_{NV2310} to 0.90, and $LRV_{Turbidity}$ to 0.95. In cases where an intact fiber was substituted with short fiber, a more significant increase in water permeability – approximately 20 % - was observed, rising to 900.4 L m^{-2} h^{-1}.bar^{-1}, while LRV_{NV2247} decreased to 0.52 and LRV_{NV2310} to 0.47, with the $LRV_{Turbidity}$ decreasing to 0.78.

When three intact fibers were replaced with short fibers, permeability increased further to 1201.3 L m^{-2} h^{-1}.bar^{-1}, representing a 60 % increase. This was accompanied by a corresponding decline in LRV_{NV2247} to 0.33 log, LRV_{NV2310} to 0.28 log, and $LRV_{Turbidity}$ to 0.37. Such a significant decline in performance indicates that fiber damage allowed unfiltered feed to enter the permeate.

When fiber damage occurs, either a portion or the entire feed flow can discharge directly to the permeate side. The tested and calculated values are summarized in Table 2. For a leaky fiber with a 0.5 mm hole, the mean velocity increased to 1.33 m/s, more than ten times higher than that of the intact fiber. Despite the increased flow, the flow remained laminar (Re = 1058.9), allowing for interaction time between the intact part of the fiber and the feed water. A friction factor dropping to 0.06 indicated reduced resistance within the fiber, allowing water bypass and increasing the permeate concentration.

For the short fiber, assuming half the length of the fiber was cut off, the flow rate increased 25-fold compared to the intact fiber. The mean velocity was 3.26 m/s, pushing the flow into a transitional regime (Re = 2603.1), signifying the onset of turbulent flow. This allowed for a near unimpeded flow of unfiltered water through the fiber. This single-fiber performance underscores the critical importance of maintaining the integrity of each fiber within the entire module.

3.2. Impact of fiber damage and replugging in pilot-scale UF module

In this pilot study, an 8" UF membrane module containing 18360 fibers (X-Flow Aquaflex 64) was investigated. The membrane performance was assessed by the retention of two NV markers and reduced turbidity. As shown in Fig. 4, the results show a high sensitivity of virus rejection to the number of damaged fibers.

Statistical analysis of the data revealed a strong negative correlation between the number of broken fibers and LRV for both NV2247 and NV2310 (Pearson correlation coefficient r = −0.9215, p = 0.0009), confirming the significant impact of fiber integrity on virus rejection. The p-value <0.05 indicates a statistically significant correlation, while

Table 2
Flow through fibers under different integrity conditions measured for 1 fiber.

Parameter	Intact fiber	Leaky fiber (0.5 mm hole)	Short fiber (half-length)
Flow rate (L/h)	0.22	2.40	5.90
Mean Velocity (m/s)	0.12	1.33	3.26
Reynolds number (Re)	99.08	1058.91	2603.16
Frictional coefficient (f)	0.65	0.06	0.03
Pressure drop (Δp, bar)	0.01	0.18	0.31

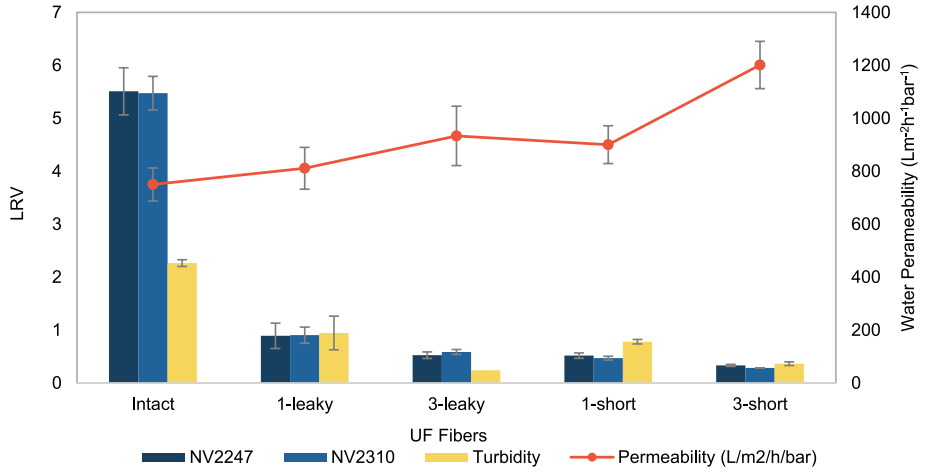

Fig. 3. Experimental data for NV marker and turbidity retention with the TRX module using the RX300 module under various integrity conditions, along with predicted LRV decline estimates from the model.

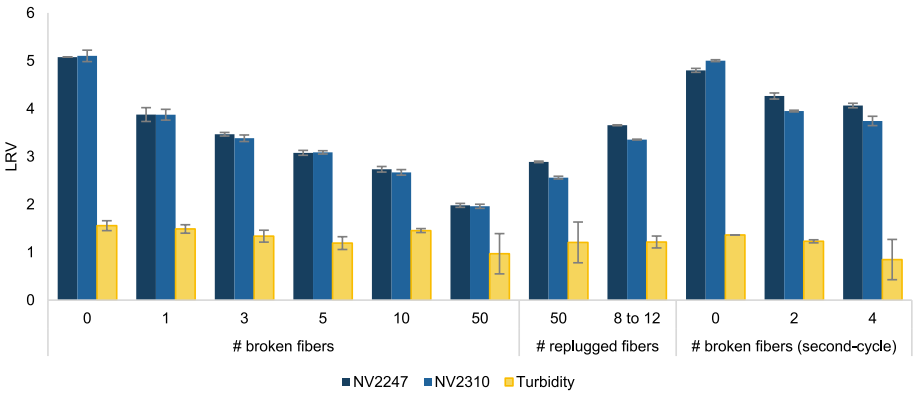

Fig. 4. Pilot study data for NV marker and turbidity retention for UF module with 18630 fibers under various integrity conditions.

the Pearson correlation coefficient, ranging from −1 to 1, reflects a negative relationship.

The presence of a single broken fiber caused a significant decrease in virus retention, with LRV_{NV2247} decreasing from 5.08 to 3.88 (a 16-fold increase in passage), and LRV_{NV2310} from 5.10 to 3.87 (a 17-fold increase in passage). In contrast, turbidity rejection remained relatively stable, decreasing only from 1.56 to 1.49.

As the number of damaged fibers increased, the LRV continued to decrease substantially. For instance, with three additional broken fibers, LRV_{NV2247} decreased to 3.47 (a 16-fold increase in the passage from the intact fiber value), and LRV_{NV2310} decreased to 3.88 (a 17-fold increase in the passage). Turbidity was less affected, decreasing from 1.55 to 1.34. In cases of more extensive damage, such as with 50 broken fibers, the LRV_{NV2247} decreased to 1.98, and LRV_{NV2310} decreased to 1.96, representing an overall increase in the passage by 128-fold and 139-fold. Turbidity rejection decreased from 0.55 to 0.97, a 1.6-fold increase in passage.

Following fiber replugging, a full recovery in membrane performance was observed. Replugging 50 damaged fibers restored approximately 46 % of the initial LRV for both the NV markers and complete recovery was achieved after further replugging. A controlled second cycle of fiber damage confirmed that damage involving 5–10 broken fibers critically impacted virus rejection, underscoring the importance of early intervention.

The results also show that turbidity measurements were less sensitive to fiber damage compared to the NV markers, particularly when the number of broken fibers was low. However, turbidity proved effective in detecting significant membrane breaches (>50 damaged fibers) suggesting it should not be relied upon as the sole indicator of virus rejection.

3.3. LRV prediction versus LRV experimental

The permeability data collected from the pilot-scale study was used to predict LRV calculations based on Eq (6) for the number of damaged fibers (N_d) ranging from 0 to 50. It was assumed that LRV = 0 applied to a broken fiber and LRV = 5 to an intact fiber (based on experimental data), leading to a total flow through the module that was a combination of flow from the damaged fiber and the intact fibers.

Fig. 5 shows the relationship between the number of damaged fibers and the predicted LRV according to the model, with an NLS fit (Root Mean Square Error (RMSE) of 0.0892) applied to the data points. The graph shows a steep decline in LRV as the number of damaged fibers increases, particularly in the range of 0–10 damaged fibers. After this initial sharp decline, the curve levels off, indicating a more gradual decrease in LRV. This nonlinear fit effectively demonstrates how even a small number of damaged fibers can significantly impact the overall LRV. Consequently, this model serves as a quantitative tool to predict the number of damaged fibers when the LRV of a full-scale system is known.

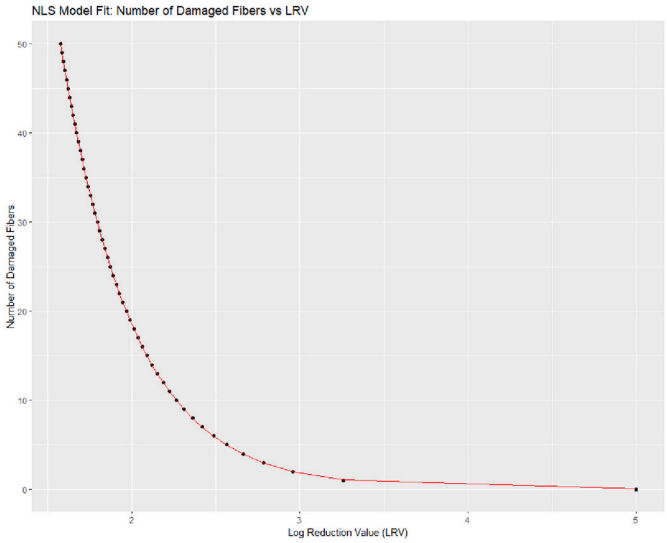

Fig. 5. Relationship between the number of damaged fibers and predicted LRV. The red line is the NLS fit made to the predicted data point. (For interpretation of the references to colour in this figure legend, the reader is referred to the Web version of this article.)

Additionally, the prediction model was compared to the experiment model, as shown in Fig. 6. An exponential fit line was plotted through the data points, indicating a strong correlation between the predicted and experimental values. The model proved to be fairly accurate in estimating the decline in LRV for the damaged fibers, closely aligning with the experimental data. To validate the choice of an exponential model over a linear fit, a residual analysis was performed (see Figure S-4).

To further support the relationship between the number of broken fibers and LRV, a change—point analysis was carried out with the LRV values obtained from the prediction model (Figure S-5). This method identified two key breakpoints where the slope of the graph changes: at 1–2 broken fiber and the second at 10 broken. Based on the statistical analysis and experimental data, we propose a threshold system for membrane modules with 18360 fibers.

- Optimal Performance (0 broken fibers): LRV ≥5.0
- Transition Zone (1–2 broken fibers): 3.3 ≥ LRV >2.9
- Compromised Performance (2–10 broken fibers): 2.9 ≥ LRV >2.3
- Critical Performance (>10 broken fibers): LRV ≤2.3

An LRV of 2.3 emerged as a Critical Performance threshold, below

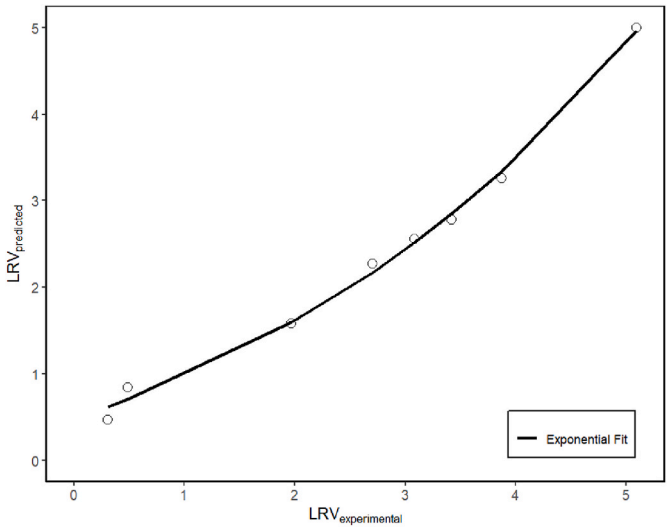

Fig. 6. Comparison of predicted LRV with experimentally obtained LRV for lab and pilot scale(n = 0,1,3,5,10,50).

which virus rejection was reduced by 55 % or more from Optimal Performance. This threshold was reached for this module with approximately 10 broken fibers, marking the transition to Critical Performance and indicating potential intervention to maintain membrane integrity through repair or replugging. When LRV decreased to below 2, observed with 50 broken fibers, an overall reduction of about 66 % in virus rejection was noted, indicating that membrane replacement might become necessary.

These thresholds have important implications for UF membrane operation and maintenance of UF membranes in full-scale scenarios. They highlight the need for advanced monitoring techniques beyond conventional methods such as turbidity measurements, particularly in the compromised performance range. The results suggest that a timely replugging strategy could potentially extend membrane lifespan by achieving full performance recovery, especially when intervention occurs before reaching the Critical Performance Stage.

3.4. Full-scale plant

The full-scale study evaluated the virus removal efficiency of UF modules across three skids, with sampling conducted from December 2020 to December 2021, focusing on the rejection of the NV2310 marker. The initial LRV_{NV2310} were 3.7 (skid 1), 3.2 logs (skid 2), and 4.1 (skid 3), establishing a baseline for evaluating skid performance throughout the study (see Fig. 7).

During the second sampling period in March 2021, skid 1 and skid 3 experienced a significant decline in virus retention, dropping to approximately LRV 2, while skid 2 maintained an LRV_{NV2310} of 3.3. By June 2021, the LRV_{NV2310} in skid 1 and skid 3 improved, reaching values between 3 and 3.5, whereas skid 2's performance worsened, falling below 2 logs. From June 2021 to December 2021, skid 3 consistently achieved LRV_{NV2310} values between 3 and 4 logs. In contrast, skids 1 and 2 continued to show unusually low virus retention, with values as low as LRV_{NV2310} 1.8. By the end of December 2021, UF modules in skids 1 and 2 were sporadically replaced with new modules, resulting in a significant recovery, boosting LRV_{NV2310} to 5.

Since all skids used the same X-flow Aquaflex 40 membranes, similar rejection values were anticipated during the sampling period under normal operational conditions. However, the deviations observed in the study, along with the data following membrane replacement, suggested that additional factors were influencing virus rejection beyond membrane pore size. The performance of the first two skids was atypical, exhibiting lower virus rejection than expected, with no signs of recovery throughout the sampling period. According to the size exclusion mechanism, high virus rejection would typically be expected in UF membranes due to their pore size concerning virus size (20 nm vs 100 nm). While the variation in skid 3 retention could be attributed to reversible fouling addressed through operational cleaning protocols, the persistent underperformance of skids 1 and 2 highlighted the complexity of factors contributing to variations in skid performance.

Water quality can significantly influence virus-membrane interaction through mechanisms such as fouling or pore blockage, while the concentration of viruses in the feed can impact virus-virus aggregation. Variations in virus concentration often occur based on geographic location and seasonal factors, leading to fluctuations in the observed LRVs of the membranes. Jacquet et al. [44] highlighted the profound effect of virus concentration on virus retention, noting that higher virus concentrations in feedwater can lead to larger viral aggregates, enhancing the size exclusion mechanism.

For example, during the first sampling in December 2020, the NV2310 feed concentration was 10^6 gene copies/mL, which increased to 10^7 gene copies/mL in the second sampling in March 2021. Despite this increase, skid 1's LRV decreased from 3.7 to 2. Increased virus concentrations often require more frequent backwashing and membrane cleaning, both of which can affect membrane structure and performance. This includes potential material degradation from cleaning chemicals or structural damage from operation conditions, leading to increased fiber movement and frictional breakage.

Several studies have indicated that water components can dictate the dominant interactions near the membrane surface, whether through size exclusion or electrostatic repulsion [45,46]. Characteristics of the feed water, such as ionic composition, high turbidity, and organic matter, can contribute to membrane fouling through pore clogging, pore size

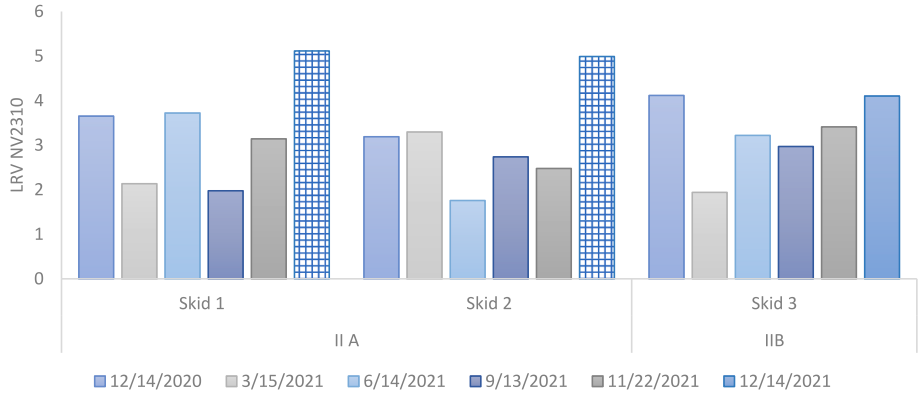

Fig. 7. LRV NV2310 of UF-unit II installation at the De Gavers WPC. The unit is split into two sections IIA, containing 3 skids with Pentair modules, and IIB with one skid of Suez modules. The checkered bars represent newly replaced modules.

diminution, or cake layer formation, thereby increasing the virus retention [47–49]. However, the feedwater in this study was not of particularly low quality, unlike raw groundwater and operational maintenance ensured regular membrane cleaning. Thus, it is likely that the decline in skid 2's performance decline was primarily due to loss of membrane integrity rather than water quality alone.

Membrane aging emerged as a key factor in the declining LRV values observed in skids 1 and 2. As membranes age, the risk of fiber breakage increases, leading to the dominance of convective transport of viruses, which bypasses static or size-related interactions with the membrane surface. This seems to be the case for skid 1 and skid 2, where the modules had already experienced a loss of integrity before the sampling period began and further deteriorated during the subsequent year of operation. The predictive model from the study indicated that one to three fibers were broken in both skids 1 and 2. The subsequent replacement of these modules with newer X-Flow Aquaflex 64 membranes resulted in a significant recovery of LRV, further supporting the hypothesis that fiber breakage was a key cause of performance decline.

Given that the WPC had been in operation for 10 years before this study, these findings align with research by Gijsbertsen-Abrahamse et al. [16], which reported that, on average, 1 out of 100,000 fibers break annually, often going undetected. These results emphasize the risk of compromised permeate water quality due to undetected fiber breakage. Unfortunately, conducting an autopsy of the modules was not feasible, which could have further substantiated the connection between performance deterioration and broken fibers as a primary factor.

Comparing these full-scale results with the thresholds established validates the system. Skid 3's performance predominantly remained within the Transition Zone to near-optimal Performance range (LRV 2.9–4.1). Skids 1 and 2 showed more variable performance, with LRV values fluctuating between 2.0 and 3.7, periodically dropping into the 'Critical Performance' range (LRV <2.3), suggesting significant fiber damage. The recovery to LRV 5 after module replacement in Skids 1 and 2 corroborates the thresholds established in Section 3.3.

It is important to note that while new UF membranes initially exhibit high LRVs (LRV_{NV2310} of 5), they are expected to stabilize at around 4 due to irreversible fouling representing a complex interplay of factors. While fouling can potentially enhance virus rejection through pore constriction and cake-enhanced concentration polarization layer formation, it may also create heterogeneities in the membrane structure and alter flow patterns [50] (F. [51]). The balance of these effects typically results in a slight decrease from the initial high LRV of new membranes but still maintains a high level of virus rejection.

4. Conclusions

This study identified fiber damage as a critical factor significantly impacting membrane performance, particularly regarding virus rejection and water permeability. The NV method demonstrated that even a small number of damaged fibers could lead to a substantial decrease in LRV, while under intact conditions, LRV 5 was observed across all measurement scales. Turbidity measurements were found to be less sensitive to fiber damage compared to virus markers, especially when only a low number of fibers were broken.

A predictive model, developed and validated against experimental data, effectively estimated the decline in LRV due to the number of damaged fibers. Both laboratory and pilot scale experiments confirmed that a single broken fiber could result in dominant convective transport of viruses, consistent with model predictions and observation from full-scale plants. This model offers a valuable tool for assessing membrane performance in real-world applications.

In full-scale operations, membrane aging and fiber breakage emerged as key factors to declining LRV values, with as few as one to three broken fibers significantly performing deterioration. These findings underscore the importance of regular monitoring and maintenance of UF membranes, as undetected fiber breakage can compromise permeate water quality. The study established threshold LRV values for decision-making in membrane maintenance: when LRV falls between 2.9 and 2.3 (Compromised Performance), fiber replugging should be considered. An LRV below 2.3 (Critical Performance) indicates the need for membrane module replacement, as demonstrated by the significant performance recovery observed after module replacement in underperforming skids during the full-scale study.

Overall, these results emphasize the necessity of implementing advanced monitoring techniques. Ultimately, the findings highlight that timely intervention – whether through repair, replugging, or replacing damaged fibers - can help maintain membrane integrity and extend the lifespan of UF systems in water treatment plants, thereby ensuring more effective and reliable water purification processes.

CRediT authorship contribution statement

Dwani Venkataswamy Gowda: Writing – original draft, Visualization, Validation, Methodology, Investigation, Formal analysis, Data curation, Conceptualization. **Danny Harmsen:** Writing – review & editing, Supervision, Methodology, Investigation. **Stefan Koel:** Resources, Methodology, Investigation. **Han Vervaeren:** Writing – review & editing, Resources. **Arnout D'Haese:** Writing – review & editing, Supervision, Funding acquisition. **Emile R. Cornelissen:** Writing – review & editing, Supervision, Resources, Project administration, Conceptualization.

Declaration of competing interest

The authors declare that they have no known competing financial interests or personal relationships that could have appeared to influence the work reported in this paper.

Acknowledgments

The author would like to acknowledge the Research Foundation – Flanders (FWO) for the financial support. This activity is co-financed with PPS funding from the Topconsortia for Knowledge & Innovations (TKI's) of the Ministry of Economic Affairs and Climate, the Netherlands.

Appendix A. Supplementary data

Supplementary data to this article can be found online at https://doi.org/10.1016/j.memsci.2025.123725.

Data availability

The authors do not have permission to share data.

References

[1] UNESCO World Water Assessment Programme, UNITED NATIONS WORLD WATER DEVELOPMENT REPORT 2023 : Partnerships and Cooperation for Water, UNITED NATIONS, 2023.
[2] Unicef, Strategy for Water, Sanitation and Hygiene 2016-2030, 2016.
[3] G. Who, UN-water Global Analysis and Assessment of Sanitation and Drinking-Water (GLAAS) Strategy, 2023, pp. 2023–2030.
[4] M.S. Islam, M. Hassan-uz-Zaman, M.S. Islam, J.D. Clemens, N. Ahmed, Waterborne pathogens, in: Waterborne Pathogens: Detection and Treatment, Elsevier, 2020, pp. 43–56, https://doi.org/10.1016/B978-0-12-818783-8.00003-7.
[5] R. Pavithra, S. Bhuvaneshwari, K. Prakash, R. Jegankumar, G. Mathan, *Geostatistical Study on waterborne disease Outbreak in India [2011–2020]*. 45–69. https://doi.org/10.1007/978-981-19-7230-0_4, 2023.
[6] M.D. Sharma, P. Mishra, A. Ali, P. Kumar, P. Kapil, R. Grover, R. Verma, A. Saini, S. Kulshrestha, Microbial waterborne diseases in India: status, interventions, and future perspectives, in: Current Microbiology, vol. 80, Springer, 2023, https://doi.org/10.1007/s00284-023-03462-2, 12.
[7] A. Cassini, E. Colzani, P. Kramarz, M.E. Kretzschmar, J. Takkinen, Impact of food and water-borne diseases on European population health, in: Current Opinion in

Food Science, vol. 12, Elsevier Ltd, 2016, pp. 21–29, https://doi.org/10.1016/j.cofs.2016.06.002.
[8] S.E. Hrudey, E.J. Hrudey, Common themes contributing to recent drinking water disease outbreaks in affluent nations, Water Sci. Technol. Water Supply 19 (6) (2019) 1767–1777, https://doi.org/10.2166/ws.2019.051.
[9] S. Hyllestad, A. Iversen, E. MacDonald, E. Amato, B.A.S. Borge, A. Boe, A. Sandvin, L.T. Brandal, T.M. Lyngstad, U. Naseer, K. Nygard, L. Veneti, L. Vold, Large waterborne Campylobacter Outbreak: use of multiple approaches to investigate contamination of the drinking water supply system, Norway, June 2019, in: Eurosurveillance, vol. 25, European Centre for Disease Prevention and Control (ECDC), 2020, https://doi.org/10.2807/1560-7917.ES.2020.25.35.2000011, 35.
[10] C. Jacqueline, M. del Valle Arrojo, P. Bellver Moreira, M.A. Rodríguez Feijóo, M. Cabrerizo, M.D. Fernandez-Garcia, Norovirus GII.3[P12] outbreak associated with the drinking water supply in a rural area in galicia, Spain, 2021, Microbiol. Spectr. 10 (4) (2022), https://doi.org/10.1128/spectrum.01048-22.
[11] European Parliament, C. of the E. U., Directive 2000/60/EC of the European Parliament and of the Council of 23 October 2000 Establishing a Framework for Community Action in the Field of Water Policy, 2000.
[12] O. Ferrer, S. Casas, C. Galvañ, F. Lucena, A. Bosch, B. Galofré, J. Mesa, J. Jofre, X. Bernat, Direct ultrafiltration performance and membrane integrity monitoring by microbiological analysis, Water Res. 83 (2015) 121–131, https://doi.org/10.1016/j.watres.2015.06.039.
[13] T. Krahnstöver, R. Hochstrat, T. Wintgens, Comparison of methods to assess the integrity and separation efficiency of ultrafiltration membranes in wastewater reclamation processes, J. Water Proc. Eng. 30 (June 2018) (2019) 100646, https://doi.org/10.1016/j.jwpe.2018.06.008.
[14] R.M. Moattari, T. Mohammadi, S. Rajabzadeh, H. Dabiryan, H. Matsuyama, Reinforced hollow fiber membranes: a comprehensive review, in: Journal of the Taiwan Institute of Chemical Engineers, vol. 122, Taiwan Institute of Chemical Engineers, 2021, pp. 284–310, https://doi.org/10.1016/j.jtice.2021.04.052.
[15] H. Yu, X. Li, H. Chang, Z. Zhou, T. Zhang, Y. Yang, G. Li, H. Ji, C. Cai, H. Liang, Performance of hollow fiber ultrafiltration membrane in a full-scale drinking water treatment plant in China: a systematic evaluation during 7-year operation, J. Membr. Sci. 613 (June) (2020) 118469, https://doi.org/10.1016/j.memsci.2020.118469.
[16] A.J. Gijsbertsen-Abrahamse, E.R. Cornelissen, J.A.M.H. Hofman, Fiber failure frequency and causes of hollow fiber integrity loss, Desalination 194 (1–3) (2006) 251–258, https://doi.org/10.1016/j.desal.2005.11.010.
[17] Z. Cui, H. Hao Ngo, Z. Cheng, H. Zhang, W. Guo, X. Meng, H. Jia, J. Wang, Hysteresis effect on backwashing process in a submerged hollow fiber membrane bioreactor (MBR) applied to membrane fouling mitigation, Bioresour. Technol. 300 (2020), https://doi.org/10.1016/j.biortech.2019.122710.
[18] E. Zondervan, A. Zwijnenburg, B. Roffel, Statistical analysis of data from accelerated ageing tests of PES UF membranes, J. Membr. Sci. 300 (1–2) (2007) 111–116, https://doi.org/10.1016/j.memsci.2007.05.015.
[19] B. Pellegrin, R. Prulho, A. Rivaton, S. Thérias, J.L. Gardette, E. Gaudichet-Maurin, C. Causserand, Multi-scale analysis of hypochlorite induced PES/PVP ultrafiltration membranes degradation, J. Membr. Sci. 447 (2013) 287–296, https://doi.org/10.1016/j.memsci.2013.07.026.
[20] Q. Li, K. Kim, S. Joag, J. Safarik, K.P. Ishida, Y.-S. Hu, Y.-X. Huang, S. Chellam, Indirect evidence that colloidal deposition inside a hollow fiber ultrafiltration membrane exacerbated fouling during municipal wastewater reclamation, ACS ES&T Eng. (2023), https://doi.org/10.1021/acsestengg.3c00402.
[21] H.E. Wray, R.C. Andrews, P.R. Bérubé, Surface shear stress and retention of emerging contaminants during ultrafiltration for drinking water treatment, Separ. Purif. Technol. 122 (2014) 183–191, https://doi.org/10.1016/j.seppur.2013.11.003.
[22] K. Farahbakhsh, D.W. Smith, Estimating air diffusion contribution to pressure decay during membrane integrity tests, J. Membr. Sci. 237 (1–2) (2004) 203–212, https://doi.org/10.1016/j.memsci.2004.03.015.
[23] S.S. Adham, J.G. Jacangelo, J.-M. Laîné, Low-pressure membranes: assessing integrity, in: Journal (American Water Works Association), vol. 87, 1995. Issue 3.
[24] N. Randles, Large scale operating experience in membrane for water and waste water reclamation, Desalination 108 (1996) 205–211.
[25] T. Krahnstöver, R. Hochstrat, T. Wintgens, Comparison of methods to assess the integrity and separation efficiency of ultrafiltration membranes in wastewater reclamation processes, J. Water Proc. Eng. 30 (February 2018) (2019) 100646, https://doi.org/10.1016/j.jwpe.2018.06.008.
[26] G.F. Crozesa, S. Sethib, B. Mi, J. Curl, B. Marifias, Improving membrane integrity monitoring indirect methods to reduce plant downtime and increase microbial removal credit, Desalination 149 (2002) 493–497. www.elsevier.com/locate/desal.
[27] Q. Wu, Z. Zhang, G. Cao, X. Zhang, Impact of polymeric membrane breakage on drinking water quality and an online detection method of the breakage, J. Environ. Sci. Health - Part A Toxic/Hazardous Substances Environ. Eng. 52 (12) (2017) 1126–1132, https://doi.org/10.1080/10934529.2017.1342496.
[28] M.E. Walsh, M.P. Chaulk, G.A. Gagnon, A.M.E. Walsh, Indirect integrity testing on a pilot-scale UF membrane. http://iwaponline.com/aqua/article-pdf/54/2/105/402593/105.pdf, 2005.
[29] J. Wang, C. Xin, J. Li, L. Song, H. Jia, Micro-bubbles enhanced breakage warning for hollow fiber membrane integrity with a low-cost real-time monitoring device, Environ. Sci. Pollut. Control Ser. 25 (25) (2018) 24639–24652, https://doi.org/10.1007/s11356-018-2415-2.
[30] V. Gitis, A. Adin, A. Nasser, J. Gun, O. Lev, Fluorescent dye labeled bacteriophages-a new tracer for the investigation of viral transport in porous media: 1. Introduction and characterization, in: Water Research, vol. 36, 2002.
[31] V. Gitis, R.C. Haught, R.M. Clark, J. Gun, O. Lev, Application of nanoscale probes for the evaluation of the integrity of ultrafiltration membranes, J. Membr. Sci. 276 (1–2) (2006) 185–192, https://doi.org/10.1016/j.memsci.2005.09.055.
[32] H. Guo, Y. Wyart, J. Perot, F. Nauleau, P. Moulin, Application of magnetic nanoparticles for UF membrane integrity monitoring at low-pressure operation, J. Membr. Sci. 350 (1–2) (2010) 172–179, https://doi.org/10.1016/j.memsci.2009.12.025.
[33] H. Guo, Y. Wyart, J. Perot, F. Nauleau, P. Moulin, Low-pressure membrane integrity tests for drinking water treatment: a review, in: Water Research, vol. 44, Elsevier Ltd, 2010, https://doi.org/10.1016/j.watres.2009.09.032. Issue 1.
[34] M.L. Pype, B.C. Donose, L. Martí, D. Patureau, N. Wery, W. Gernjak, Virus removal and integrity in aged RO membranes, Water Res. (2016), https://doi.org/10.1016/j.watres.2015.12.023.
[35] C. Xin, J. Wang, H. Jia, H. Wen, J. Li, Hollow fiber membrane integrity warning device based on laser extinction particles detection technology, Separ. Purif. Technol. 224 (2019) 295–303, https://doi.org/10.1016/j.seppur.2019.05.045.
[36] L.M. Hornstra, B. Blankert, L. Heijnen, E. Beerendonk, R. Cornelissen, G. Medema, Environmental Science viruses and bacteriophages, 1535–1544, https://doi.org/10.1039/c9ew00318e, 2019.
[37] P. Cote, Z. Alam, J. Penny, Hollow fiber membrane life in membrane bioreactors (MBR), Desalination 288 (2012) 145–151, https://doi.org/10.1016/j.desal.2011.12.026.
[38] L.M. Hornstra, T. Rodrigues Da Silva, B. Blankert, L. Heijnen, E. Beerendonk, E. R. Cornelissen, G. Medema, Monitoring the integrity of reverse osmosis membranes using novel indigenous freshwater viruses and bacteriophages, Environmental Science: Water Res. Technol. 5 (9) (2019) 1535–1544, https://doi.org/10.1039/c9ew00318e.
[39] J. Cromphout, J. Coemelck, W. Closset, L. Verdickt, Design and operation of an ultrafiltration plant for the production of drinking water out of the river Scheldt. https://www.researchgate.net/publication/285778093, 2011.
[40] H. Schlichting, K. Gersten, Boundary-layer theory, in: Boundary-Layer Theory, Springer Berlin Heidelberg, 2016, https://doi.org/10.1007/978-3-662-52919-5.
[41] A. Lidén, E. Lavonen, K.M. Persson, M. Larson, Integrity breaches in a hollow fiber nanofilter – effects on natural organic matter and virus-like particle removal, Water Res. 105 (2016) 231–240, https://doi.org/10.1016/j.watres.2016.08.056.
[42] H. Schlichting, K. Gersten, Boundary-layer Theory, springer, 2016.
[43] S. Giglia, M. Krishnan, High sensitivity binary gas integrity test for membrane filters, J. Membr. Sci. 323 (1) (2008) 60–66, https://doi.org/10.1016/j.memsci.2008.06.017.
[44] N. Jacquet, S. Wurtzer, G. Darracq, Y. Wyart, L. Moulin, P. Moulin, Effect of concentration on virus removal for ultrafiltration membrane in drinking water production, J. Membr. Sci. 634 (January) (2021) 119417, https://doi.org/10.1016/j.memsci.2021.119417.
[45] A.M. Elhadidy, S. Peldszus, M.I. Van Dyke, An evaluation of virus removal mechanisms by ultrafiltration membranes using MS2 and φx174 bacteriophage, Separ. Purif. Technol. 120 (2013) 215–223, https://doi.org/10.1016/j.seppur.2013.09.026.
[46] G.J. Gentile, M.C. Cruz, V.B. Rajal, M.M. Fidalgo de Cortalezzi, Electrostatic interactions in virus removal by ultrafiltration membranes, J. Environ. Chem. Eng. 6 (1) (2018) 1314–1321, https://doi.org/10.1016/j.jece.2017.11.041.
[47] S. Lee, M. Ihara, N. Yamashita, H. Tanaka, Improvement of virus removal by pilot-scale coagulation-ultrafiltration process for wastewater reclamation: effect of optimization of pH in secondary effluent, Water Res. 114 (2017) 23–30, https://doi.org/10.1016/j.watres.2017.02.017.
[48] Z. Ren, H. Cao, P. Desmond, B. Liu, H.H. Ngo, X. He, G. Li, J. Ma, A. Ding, Ions play different roles in virus removal caused by different NOMs in UF process: removal efficiency and mechanism analysis, Chemosphere 313 (2023), https://doi.org/10.1016/j.chemosphere.2022.137644.
[49] Z. Yin, V.V. Tarabara, I. Xagoraraki, Human adenovirus removal by hollow fiber membranes: effect of membrane fouling by suspended and dissolved matter, J. Membr. Sci. 482 (2015) 120–127, https://doi.org/10.1016/j.memsci.2015.02.028.
[50] A. Antony, J. Blackbeard, G. Leslie, Removal efficiency and integrity monitoring techniques for virus removal by membrane processes, Crit. Rev. Environ. Sci. Technol. 42 (9) (2012) 891–933, https://doi.org/10.1080/10643389.2011.556539.
[51] F. Wang, V.V. Tarabara, Pore blocking mechanisms during early stages of membrane fouling by colloids, J. Colloid Interface Sci. 328 (2) (2008) 464–469, https://doi.org/10.1016/j.jcis.2008.09.028.